Environmental Pollution 247 (2019) 907–916

Contents lists available at ScienceDirect

Environmental Pollution

journal homepage: www.elsevier.com/locate/envpol

Co-transport of multi-walled carbon nanotubes and sodium dodecylbenzenesulfonate in chemically heterogeneous porous media☆

Miaoyue Zhang [a, b, *], Scott A. Bradford [c], Jirka Šimůnek [d], Harry Vereecken [b], Erwin Klumpp [b]

[a] School of Environmental Science and Engineering, Sun Yat-sen University, 510006, Guangzhou, PR China
[b] Agrosphere Institute (IBG-3), Forschungszentrum Jülich GmbH, 52425, Jülich, Germany
[c] United States Department of Agriculture, Agricultural Research Service, U. S. Salinity Laboratory, Riverside, CA, 92507, USA
[d] Department of Environmental Sciences, University of California Riverside, Riverside, CA, 92521, USA

ARTICLE INFO

Article history:
Received 4 September 2018
Received in revised form
20 January 2019
Accepted 26 January 2019
Available online 1 February 2019

Keywords:
Multi-walled carbon nanotubes
Sodium dodecylbenzenesulfonate
Competitive blocking
Breakthrough curves
Retention profiles
Modeling

ABSTRACT

Multi-walled carbon nanotubes (MWCNTs) are increasing used in commercial applications and may be released into the environment with anionic surfactants, such as sodium dodecylbenzenesulfonate (SDBS), in sewer discharge. Little research has examined the transport, retention, and remobilization of MWCNTs in the presence or absence of SDBS in porous media with controlled chemical heterogeneity, and batch and column scale studies were therefore undertaken to address this gap in knowledge. The adsorption isotherms of SDBS on quartz sand (QS), goethite coated quartz sand (GQS), and MWCNTs were determined. Adsorption of SDBS (MWCNTs » GQS > QS) decreased zeta potentials for these materials, and produced a charge reversal for goethite. Transport of MWCNTs (5 mg L^{-1}) dramatically decreased with an increase in the fraction of GQS from 0 to 0.1 in the absence of SDBS. Conversely, co-injection of SDBS (10 and 50 mg L^{-1}) and MWCNTs radically increased the transport of MWCNTs when the GQS fraction was 0, 0.1, and 0.3, especially at a higher SDBS concentration, and altered the shape of retention profile. Mathematical modeling revealed that competitive blocking was not the dominant mechanism for the SDBS enhancement of MWCNT transport. Rather, SDBS sorption increased MWCNT transport by increasing electrostatic and/or steric interactions, or creating reversible interactions on rough surfaces. Sequential injection of pulses of MWCNTs and SDBS in sand (0.1 GQS fraction) indicated that SDBS could mobilize some of retained MWCNTs from the top to deeper sand layers, but only a small amount of released MWCNTs were recovered in the effluent. SDBS therefore had a much smaller influence on MWCNT transport in sequential injection than in co-injection, presumably because of a greater energy barrier to MWCNT release than retention. This research sheds novel insight on the roles of competitive blocking, chemical heterogeneity and nanoscale roughness, and injection sequence on MWCNT retention and release.

1. Introduction

Carbon nanotubes (CNTs) consist of rolled-up graphene sheets (Iijima, 1991) that have been used in many commercial applications such as electrical cables and wires (Janas et al., 2014), hydrogen storage (Dillon et al., 1997), solar cells (Guldi et al., 2005), radar absorption (Lin et al., 2008), and may potentially be employed in environmental remediation (Mauter and Elimelech, 2008; Pan and Xing, 2012) and water treatment (Camilli et al., 2014; Li et al., 2012; Zhang et al., 2010). The widespread use of CNTs will undoubtedly result in their release into the environment (Gottschalk et al., 2009). Published studies have investigated the transport behavior of CNTs in porous media under various physicochemical conditions, such as solution ionic strength (IS), water content, grain size, input concentration, dissolved organic matter, and surfactants (Jaisi and

☆ This paper has been recommended for acceptance by Baoshan Xing.

* Corresponding author.School of Environmental Science and Engineering, Sun Yat-sen University, 510006, Guangzhou, PR China.
E-mail address: zhangmy53@mail.sysu.edu.cn (M. Zhang).

https://doi.org/10.1016/j.envpol.2019.01.106
0269-7491/

Elimelech, 2009; Kasel et al., 2013a; Kasel et al., 2013b; Liu et al., 2009; Lu et al., 2013; Lu et al., 2014; Yang et al., 2013; Yuan et al., 2012).

Surfactants are often used to stabilize CNT suspensions (Lu et al., 2013; Lu et al., 2014; Yu et al., 2007), and the mobility of CNTs in porous media was strongly influenced by the presence of various stabilizing agents such as sodium dodecylbenzenesulfonate (SDBS), octyl-phenolethoxylate, and cetylpyridinium chloride. However, these studies were conducted over a limited ranged in CNTs (high) and surfactant (low) input concentrations. The total concentration of surfactants that discharges in municipal sewer is about 20–70 mg L^{-1} (Matthijs et al., 1999). These surfactant concentrations are much greater than the predicted discharge of CNTs (Gottschalk et al., 2009), and may be high enough to stabilize CNT suspensions. However, little research has investigated the influence of surfactants on CNT transport when the surfactant concentration was greater than the CNT concentration. Furthermore, previous literature considered the simultaneous transport of a mixture of surfactants and CNTs, whereas the more environmentally relevant scenario of sequential release of surfactants and CNTs due to waste discharge has not yet been investigated.

Previous research with CNTs and surfactants focused on determination of breakthrough curves (BTCs), but did not measure the influence of surfactants on CNT retention profiles (RPs) (Lu et al., 2013; Lu et al., 2014). Liang et al. (2013) demonstrated that the presence of surfactants had a large influence on the shape of the RPs for silver nanoparticles in quartz sand, but little influence on their BTCs. This was attributed to competitive blocking (e.g., filling) of silver nanoparticle retention sites by surfactant. Similarly, Becker et al. (2015) showed that the stabilizing agent can compete for the same retention sites as quantum dot nanocrystals. Natural porous media often exhibit surface charge heterogeneity due to Fe and Al oxyhydroxides with a net positive surface charge (Parks, 1965) and common silica minerals with a net negative surface charge (Alvarezsilva et al., 2010) at ambient pH. Nanoparticle attachment onto positively charged sites can be inhibited by surfactant sorption which can neutralize or reverse the surface charge (Lin et al., 2012; Wang et al., 2012c). The influence of competitive blocking on CNT BTCs and RPs is therefore expected to be a function of the chemical heterogeneity of the porous medium. In the absence of surfactant, Zhang et al. (2016b) demonstrated that increasing the goethite-coated fraction of quartz sand increased the retention of CNTs due to the combined influence of surface roughness and positively charged sites. To the best of our knowledge, no research studies have examined the influence of surface roughness and controlled soil chemical heterogeneities on the transport and fate of functionalized CNTs in the presence of surfactants. Additional research is needed to assess the potentially significant influence of surfactants on competitive blocking and CNT RPs, especially in porous media with chemical heterogeneity and roughness.

The objective of this study is to better understand and quantify the role of anionic surfactant SDBS concentrations (10–50 mg L^{-1}) on the transport, retention, and remobilization behavior of functionalized multi-walled carbon nanotubes (MWCNTs, 5 mg L^{-1}) in chemically heterogeneous porous media. The sorption affinity for SDBS to quartz sand (QS), goethite-coated quartz sand (GQS), and MWCNTs was determined in batch experiments. Column experiments were employed to determine BTCs for both MWCNT and SDBS, and RPs for MWCNTs in chemically heterogeneous mixtures of QS and GQS. Kinetic retention, release, and competitive blocking parameters for MWCNTs and SDBS were determined by inverse optimization of the collected column data. Furthermore, this research sheds novel insight on the roles of competitive blocking, chemical heterogeneity and nanoscale roughness, and injection sequence on MWCNT retention and release, and the develop of MWCNT retention profiles. This knowledge can be useful for environmental applications and risk management of MWCNTs in the presence of surfactant and various amounts of soil chemical heterogeneity.

2. Materials and methods

2.1. Porous media and MWCNTs

Quartz sand (QS, 240 μm), which was used in experiments (Quarzwerke GmbH, 50226 Frechen, Germany) was purified following a protocol in the literature. The preparation of goethite-coated quartz sand (GQS) has been described in a former study (Zhang et al., 2016b). The chemically heterogeneous porous medium was prepared by combining various amounts of QS with a known mass fraction of GQS (λ, the mass ratio of GQS in the mixed porous medium; i.e., λ = 0 and 1 for a porous medium with only QS and GQS, respectively). The goethite coating was verified to be stable by measuring negligible amounts of iron (inductively coupled optical emission spectrometry, Agilent) in the effluent of a column packed with chemically heterogeneous sand (λ = 0.3) under steady-state flow and solution chemistry (1 mM KCl) conditions. Zhang et al. (2016b) examined the roughness and chemical composition of GQS using a scanning electron microscope (SEM, Supra50VP, Carl Zeiss NTS GmbH, Germany) that was equipped with energy dispersive x-ray (EDX, SDD-Detector, Oxford Instruments, UK), and determined specific surface areas of QS and GQS.

SDBS surfactant was purchased from Sigma-Aldrich Chemie GmbH (Munich, Germany). SDBS stock solutions (100 mg L^{-1}) were prepared by adding 50 mg surfactant into 500 ml Milli-Q water. The synthesis, functionalization, and characterization of radioactively (^{14}C) labeled and unlabeled MWCNTs (Bayer Technology Services GmbH, Leverkusen, Germany) were previously described by Kasel et al. (2013a,b). In brief, the morphological properties of MWCNTs was determined using a transmission electron microscope and oxygen containing functional groups were determined using X-ray photoelectron spectrometry. The MWCNTs have a median diameter of 10–15 nm and a median length of 200–1000 nm (Pauluhn, 2010), an average hydrodynamic diameter of approximately 180 nm (1 mg L^{-1}, in 1 1 mM KCl), and a specific density of 1.641 g cm^{-3}. The point of zero charge for oxidized MWCNTs has been reported by Han et al. (2008).

Stock suspension of ^{14}C-labeled MWCNTs (100 mg L^{-1}) was prepared by suspending MWCNTs in Milli-Q water and ultrasonicating for 15 min at 65 Watts using a cup horn sonicator (Branson Sonifier ® W-250, Danbury, USA). Then, stock suspension of ^{14}C-labeled MWCNTs was diluted using different SDBS concentrations (0, 10, and 50 mg L^{-1}) at the desired ionic strength (1 mM KCl). To ensure thorough dispersion, mixtures of MWCNT and SDBS were ultrasonicated for 15 min at 65 W and then ultrasonicated again for 10 min before use in characterization, batch, and column experiments discussed below.

The hydrodynamic radius does not reflect the real geometric particle diameter for non-spherical particles like MWCNTs (Hassellöv et al., 2008; Pecora, 2000). Nevertheless, it can be used for comparison of the stability of MWCNTs suspensions in the presence of surfactant. The hydrodynamic radius of the MWCNTs suspensions in 1 mM KCl at different SDBS concentrations (0, 10, and 50 mg L^{-1}) was therefore measured using a Zetasizer Nano (Malvern Instruments GmbH, 71083 Herrenberg, Germany) immediately after suspension preparation and at 1 h. The hydrodynamic radius of the MWCNTs suspensions at different SDBS concentrations (0, 10, and 50 mg L^{-1}) was 334.6, 315.1, and 306.3 nm, respectively, and in the same range at 0 and 1 h. The MWCNTs

suspensions were therefore considered to be less aggregated as SDBS concentrations increased and stable during this time interval.

The zeta potentials of MWCNTs, crushed QS, and goethite in 1 mM KCl and at different surfactant concentrations was also measured using a Zetasizer Nano. Fig. S1 of the supporting information (SI) provides results. The pH values of MWCNTs suspensions at different SDBS concentrations (0, 10, and 50 mg L^{-1}, 1 mM KCl) were measured using a pH meter (Mettler Toledo MP230 pH meter).

2.2. Determination of concentrations of MWCNTs and SDBS

Concentrations of ^{14}C-labeled MWCNT in various SDBS solutions (0–50 mg L^{-1}) were determined using a liquid scintillation counter (LSC) (PerkinElmer, Rodgau, Germany). Effluent concentrations of SDBS in batch and column experiments discussed below were measured using a UV–Vis spectrometer (Beckman DU-640, U.S.A) at a wavelength of 230 nm. However, both SDBS and MWCNTs have absorbance at a wavelength of 230 nm. Calibrations curves of absorbance and concentration of MWCNTs, SDBS, and SDBS-MWCNTs (MWCNTs modified by SDBS) were therefore established at a wavelength of 230 nm (Fig. S2). The additivity of individual absorbance of MWCNTs, SDBS, and SDBS-MWCNTs can be applied to quantitatively determine the concentrations of SDBS in the effluent. Details pertaining to these calculations are given in the section S1 of the SI.

2.3. Batch experiments

Adsorption isotherms of SDBS on QS (240 μm), GQS (240 μm, λ = 0.1 and 0.3), and MWCNTs were determined in batch trials following a published protocol (OECD, 2006). Details pertaining to these calculations are given in the section S2 of the SI.

2.4. Column transport experiments

Stainless steel columns with a 3 cm inner diameter and 12 cm length were uniformly wet packed with a selected mixture of QS and GQS (λ = 0.0, 0.1, and 0.3). The packed columns were equilibrated by flushing with approximately 30 pore volumes (PVs) of background electrolyte (1 mM KCl) solution before initiating transport experiments. In order to characterize the column's hydraulic conditions, a non-reactive tracer (1 mM KBr in 1 mM KCl) was injected into the column at a steady-state Darcy velocity of 0.71–0.73 cm min^{-1} for approximately 2.6 PVs (90 mL), followed by continued elution at the same velocity with tracer-free 1 mM KCl solution. Effluent solutions were collected using a fraction collector (FoxyJr.®, Teledyne Isco Inc., Lincoln, USA) every 30 s. The effluent concentrations of bromide were measured by using a high-performance liquid chromatograph (STH 585, Dionex, Sunnyvale, CA, USA) equipped with a UV detector (UV2075, Jasco, Essex, UK).

Following completion of the tracer experiment, the packed columns were employed to study the transport of a 2.6 PV pulse of MWCNT suspension (5 mg L^{-1}, 1 mM KCl) in the presence of various SDBS concentrations (0, 10, and 50 mg L^{-1}) through a selected chemically heterogeneous porous medium (λ = 0, 0.1, and 0.3). The same protocol was employed for tracer and MWCNT transport experiments. The effluent concentrations of MWCNTs and SDBS were determined using approaches outlined in section 2.2. After recovery of the MWCNT breakthrough curve (BTC), the MWCNT retention profile (RP) was determined by excavating sand in approximately 0.5–1 cm thick increments, drying, homogenizing using a mill, combusting using a biological oxidizer, and then measuring the MWCNT concentration with the LSC. A summary of the experimental conditions and mass balance information is provided in Table 1. All column experiments were replicated and exhibited good reproducibility.

2.5. Numerical modeling

The HYDRUS-1D computer code (Šimůnek et al., 2008) was used to simulate the transport and retention of MWCNTs and SDBS in the column experiments. The aqueous and solid phase mass balance equations for MWCNTs are given in this model as:

$$\frac{\partial C}{\partial t} = \frac{\partial}{\partial z}\left(D\frac{\partial C}{\partial z}\right) - \frac{\partial (vC)}{\partial z} - \psi k_1 C + \rho_b k_d S \quad [1]$$

$$\frac{\partial (\rho_b S)}{\partial t} = \theta_w \psi k_1 C - \rho_b k_d S \quad [2]$$

where θ_w [−] is the volumetric water content, C [N L^{-3}, N and L denote the number of MWCNTs and units of length, respectively] is the aqueous phase MWCNT concentration, t is time [T, T denotes time units], z [L] is the distance from the column inlet, D [L^2T^{-1}] is the hydrodynamic dispersion coefficient, v [LT^{-1}] is the pore-water velocity, ψ [-] is a dimensionless function to account for time- and depth-dependent blocking, k_1 [T^{-1}] is the first-order retention coefficient, k_d [T^{-1}] is the first-order detachment coefficient, ρ_b [M L^{-3}, M denote units of mass] is the soil bulk density, and S [N M^{-1}] is the solid phase MWCNT concentration. The first and second terms on the right hand side of Eq. [1] account for dispersive and

Table 1
Experimental conditions and mass recoveries from effluent for all column experiments. The ionic strength was 1 mM KCl, d_{50} = 240 μm, and the input concentration of MWCNTs was 5 mg L^{-1}.

Fig.No.	λ	Disp. [cm^2min^{-1}]	$C_{o\ (MWCNTs)}$ [mg L^{-1}]	$C_{o\ (SDBS)}$ [mg L^{-1}]	q [cm min^{-1}]	Porosity	M_{surf} [%]	M_{eff} [%]	M_{solid} [%]	M_{total} [%]
1,2	0	0.2875	5	0	0.71	0.43	NA	17.51	87.08	104.60
1,3,4	0.1	0.0708	5	0	0.73	0.44	NA	2.41	98.39	100.79
1,2	0	0.0185	0	10	0.72	0.43	95.50	NA	NA	NA
1,3	0.1	0.0195	0	10	0.72	0.43	92.77	NA	NA	NA
2,3	0	0.2875	5	10	0.72	0.42	91.55	87.18	10.20	97.38
2	0	0.0108	5	50	0.72	0.45	94.97	90.49	9.88	100.38
3	0.1	0.0708	5	10	0.73	0.41	86.37	64.22	34.90	99.12
3	0.3	0.0399	5	10	0.73	0.42	84.39	0.32	97.17	97.49
4	0.1	0.0418	5	10	0.72	0.45	80.01	2.47	97.22	99.70

Fig. No. is the number of Fig. NA denotes not applicable. λ, is the mass ratio of goethite coated quartz sand (GQS) in the porous medium; when λ = 0, the porous medium is quartz sand. *Disp.*is the estimated longitudinal dispersivity. $C_{o\ (MWCNTs)}$ and $C_{o\ (SDBS)}$ are the input concentrations of MWCNTs and SDBS, respectively. q is the Darcy velocity. M_{surf} is the effluent percentage of SDBS recovered from the column experiment. M_{eff}, M_{solid}, and M_{total} are the effluent percentage, the retained percentage, and the total percentage of MWCNTs recovered from the column experiment, respectively.

advective transport of MWCNTs, respectively. Third and forth terms in Eq. [1] are used to describe retention and release to/from the solid phase, respectively. The value of ψ is given in this work as:

$$\psi = \left(1 - \frac{S + \Gamma S_s}{S^{max}}\right)\left(\frac{d_{50} + z}{d_{50}}\right)^{-\beta} \quad [3]$$

where S_s [N_s M^{-1}; N_s denotes the number of surfactant] is the solid phase concentration of the surfactant SDBS, S^{max} [N M^{-1}] is the maximum solid phase concentrations of MWCNTs, Γ [-] is the area conversion factor between SDBS and MWCNTs, d_{50} [L] is the median sand grain diameter, and β [-] is an empirical parameter that controls that depth-dependency of the retention rate coefficient. The value of β was set to 0.765 based on our previous study with MWCNTs in chemically heterogeneous sand (Zhang et al., 2016a; Zhang et al. 2016b; Zhang et al. 2017).

Similar to the MWCNT, the aqueous and solid phase mass balance equations for the surfactant SDBS are given in this model as:

$$\frac{\partial C_s}{\partial t} = \frac{\partial}{\partial z}\left(D\frac{\partial C_s}{\partial z}\right) - \frac{\partial(vC_s)}{\partial z} - k_{1s}\psi_s C_s + \rho_b k_{ds} S_s \quad [4]$$

$$\frac{\partial(\rho_b S_s)}{\partial t} = \theta_w k_{1s}\psi_s C_s - \rho_b k_{ds} S_s \quad [5]$$

where the superscript s on parameters indicates that they are associated with the surfactant SDBS. In the absence of experimental information about the depth dependency of SDBS retention, the value of ψ_s is given as:

$$\psi_s = \left(1 - \frac{S_s + \Gamma_s S}{S_s^{max}}\right) \quad [6]$$

Eq. [3] and [6] allow for the possibility of single species and competitive Langmuirian blocking. Langmurian blocking (Adamczyk et al., 1994) is modelled using the first term on the right hand side of these equations when Γ and Γ_s are set to zero, whereas competitive blocking (Becker et al., 2015) is considered when Γ and Γ_s are greater than zero. The parameter Γ accounts for differences in the cross-sectional areas of the particles and the porous medium surface that contributes to retention of MWCNTs and SDBS. When S^{max} and S_s^{max} encompass the same area on the porous media surface, the value of $\Gamma = 1/\Gamma_s = A_s/A$ (Becker et al., 2015), where A_s [L^2] and A [L^2] are the cross-sectional areas of SDBS and MWCNT, respectively.

HYDRUS-1D includes provisions for inverse parameter estimation using a nonlinear least squares optimization routine. The bromide tracer data was simulated using the solution of the advection dispersion equation (Eq. [1] with $k_1 = 0$), and values of v and D were determined by inverse optimization. Values of k_1, k_d, and S^{max} were determined by inverse optimization to the BTC and RP for MWCNTs. Values of k_{1s}, k_{ds}, and S_s^{max} were determined by inverse optimization to the BTC for SDBS. The single-species transport (SST) of MWCNTs and SDBS were described with Eqs. [1–3] and [4–6], respectively, by setting Γ and Γ_s to zero. Three modeling approaches (denoted as M1, M2, and M3) were considered when both MWCNTs and SDBS were simultaneously present. The M1 approach neglects competitive blocking by setting Γ and Γ_s to zero, and then optimizing transport and retention parameters to MWCNT and SDBS data sets as if they were independently obtained. The M2 approach allows for a small amount of competitive blocking by fixing the retention and release parameters to those determined from M1, and then optimizing values of Γ and Γ_s to both MWCNT and SDBS data sets. The M3 approach allows for the maximum amount for competitive blocking by fixing retention and release parameters for MWCNTs and SDBS that were determined in the absence of the competitive species, and then optimizing values of Γ and Γ_s to both MWCNT and SDBS data sets.

3. Results and discussion

3.1. Adsorption of SDBS on QS, GQS and MWCNTs

The functionalization of MWCNTs produced an increased amount of groups containing oxygen (e.g. carboxylic groups) in comparison to the pristine MWCNTs (Kasel et al., 2013a; Wei et al., 2007), resulting in its negative zeta potential in 1 mM KCl solution (Fig. S1). Zeta potentials of MWCNTs, QS, and goethite decreased with increasing SDBS concentration, suggesting that the increased electrostatic repulsion from adsorbed SDBS can enhance the stability of functionalized MWCNTs. The pH of the MWCNTs suspensions slightly increased from 5.39, 5.81, and 6.42 with an increase in the SDBS concentrations of 0, 10, and 50 mg L^{-1}, respectively, due to the generation of more hydroxyls radicals (Duan et al., 2018). This variation in pH is expected to influence the interaction between MWCNTs and QS/GQS by decreasing the zeta potential of these surfaces and creating a greater energy barrier to interaction in a primary minimum (Wang et al., 2012a). Zhang et al. (2016a,b) calculated interaction energies for MWCNTs on QS and GQS surfaces with different surface roughness properties in 1 mM KCl by treated them as equivalent solid spherical particles. Small fractions of nanoscale roughness were demonstrated to play a dominant role on MWCNT interaction energies on both QS and GQS; e.g., reducing the energy barrier height and the depths of primary and secondary minima.

Adsorption isotherms of SDBS on QS, GQS, and MWCNTs are shown in Fig. S3. Adsorption of SDBS followed an order: MWCNTs » GQS > QS. It is worth noting that the adsorption affinity of SDBS on GQS increased as λ increased. That can be explained by the enhanced surface area and positive charge of goethite (e.g., Fig. S1). The adsorption isotherm initially increased sharply, then reached a plateau at an equilibrium surfactant concentration of about 5 mg L^{-1}. This behavior is consistent with observations reported by Han et al. (2008). Adsorption of SDBS on MWCNTs can be explained by hydrophobic interactions between the hydrophobic chains on the surfactant and hydrophobic sites on the MWCNTs (Matarredona et al., 2003), and the benzene ring of SDBS induces Pi-Pi interactions with MWCNTs (Tan et al., 2008). The SDBS isotherms on QS, GQS, and MWCNTs were described using Langmuir and Freundlich models (Fig. S3) with $R^2 > 0.87$. The adsorption isotherms on MWCNTs were close to High-affinity type (Fig. S3).

3.2. Single-species transport of MWCNTs and SDBS

Column experiments were performed to understand the single-species transport behavior of MWCNTs and SDBS in chemically heterogeneous porous media (λ = 0 and 0.1). The experimental conditions and mass balance information are presented in Table 1. The parameters $d_{50} = 240$ μm, IS = 1 mM KCl, and q = 0.71–0.73 cm min^{-1} were the same for all experiments. The input concentration (C_o) was 5 mg L^{-1} for MWCNTs and 10 mg L^{-1} for SDBS.

The total recovered mass from the BTCs and RPs for MWCNTs was very good (>97%). The MWCNT effluent mass balance (M_{eff}) strongly decreased from 17.5% to 2.4% (Table 1) as λ increased from 0 to 0.1. Similarly, the MWCNT retained mass balance (M_{solid}) increased from 87.1% to 98.4% as λ increased from 0 to 0.1. Observed and simulated BTCs for MWCNTs are plotted as normalized effluent concentrations (C/C_o) versus pore volumes in Fig. 1a. The BTCs were very-well described by the model ($R^2 > 0.97$), and parameters k_1 and S_{max}/C_o both increased with λ (Table 2). Blocking was clearly evident in the BTCs, whereas release was very minor ($k_d = 0.0001$

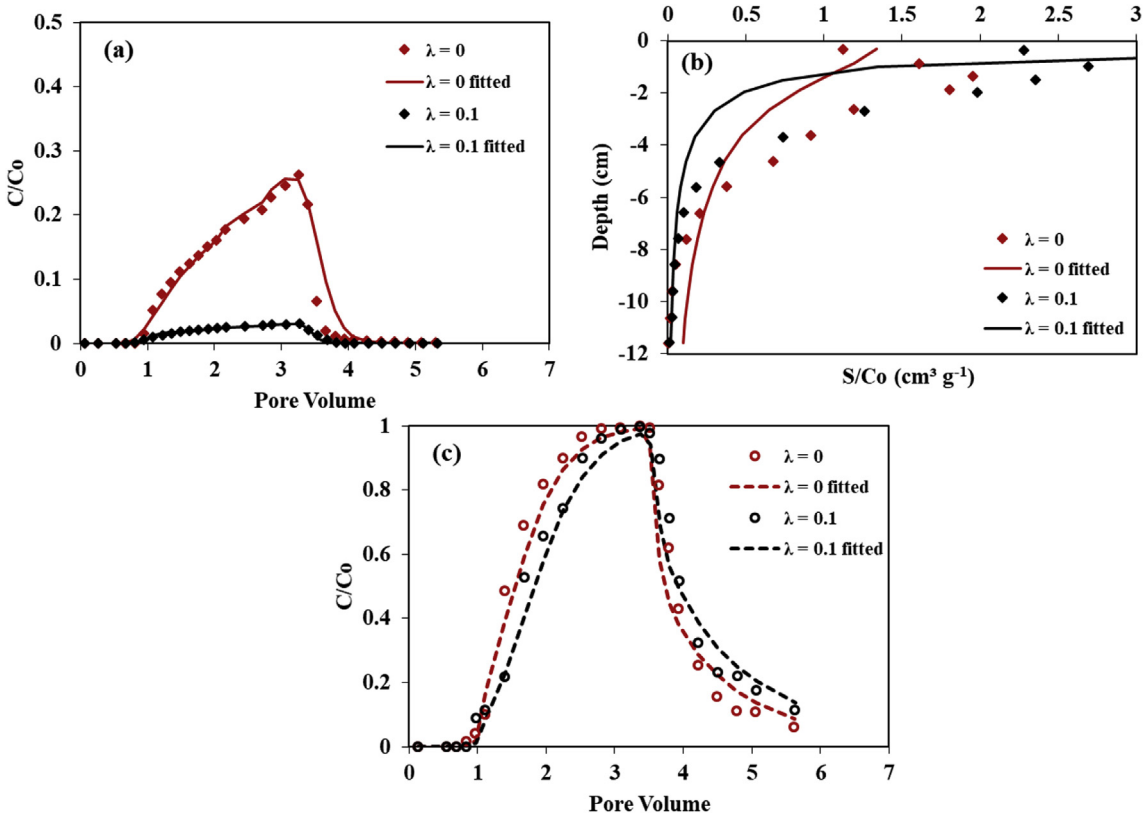

Fig. 1. Observed and fitted breakthrough curves (BTCs, a and c) and retention profiles (RPs, b) of MWCNTs and SDBS in porous media at different λ (λ, the mass ratio of goethite coated quartz sand in the porous medium). (a) BTCs of MWCNTs at λ = 0 and 0.1; (b) RPs of MWCNTs at λ = 0 and 0.1; (c) BTCs of SDBS at λ = 0 and 0.1. The input concentrations of MWCNTs and SDBS were 5 and 10 mg L^{-1}, respectively. The ionic strength was 1 mM KCl. The Darcy velocity is 0.71–0.73 cm min^{-1}.

Table 2
Fitted model parameters.

Fig. No.	*Model*	*AIC*	S^{max}/C_o [cm^3g^{-1}]	Γ [-]	k_1 [min^{-1}]	S_s^{max}/C_o [cm^3g^{-1}]	Γ_s [-]	k_{1s} [min^{-1}]	k_{ds} [min^{-1}]	R^2_{BTC}	R^2_{RP}	$R^2_{s\ BTC}$
λ = 0, $C_{o\ (MWCNTs)}$ = 5 mg L^{-1}, $C_{o\ (SDBS)}$ = 0 mg L^{-1}												
1,2	SST	−101.90	1.351	NA	13.000	NA	NA	NA	NA	0.970	0.876	NA
λ = 0.1, $C_{o\ (MWCNTs)}$ = 5 mg L^{-1}, $C_{o\ (SDBS)}$ = 0 mg L^{-1}												
1,3,4	SST	−52.95	27.450	NA	19.910	NA	NA	NA	NA	0.991	0.647	NA
λ = 0, $C_{o\ (MWCNTs)}$ = 0 mg L^{-1}, $C_{o\ (SDBS)}$ = 10 mg L^{-1}												
1,2	SST	−2.06	NA	NA	NA	0.263	NA	0.258	0.200	NA	NA	0.986
λ = 0.1, $C_{o\ (MWCNTs)}$ = 0 mg L^{-1}, $C_{o\ (SDBS)}$ = 10 mg L^{-1}												
1,3	SST	−119.90	NA	NA	NA	0.384	NA	0.362	0.200	NA	NA	0.986
λ = 0, $C_{o\ (MWCNTs)}$ = 5 mg L^{-1}, $C_{o\ (SDBS)}$ = 10 mg L^{-1}												
2,3	M1	−308.00	0.063	0.000	1.426	0.110	0.000	0.064	0.126	0.988	0.964	0.970
S4	M2	−306.10	0.063	0.002	1.426	0.110	0.031	0.064	0.126	0.988	0.964	0.970
S4	M3	−304.80	1.351	2.169	13.000	0.263	43.880	0.258	0.200	0.989	0.869	0.961
λ = 0, $C_{o\ (MWCNTs)}$ = 5 mg L^{-1}, $C_{o\ (SDBS)}$ = 50 mg L^{-1}												
2	M1	−308.40	0.061	0.000	1.377	0.090	0.000	0.061	0.163	0.987	0.944	0.977
S4	M2	−306.70	0.061	0.034	1.377	0.090	0.166	0.061	0.163	0.987	0.945	0.977
S4	M3	−167.20	1.351	47.040	13.000	0.263	151.200	0.258	0.200	0.983	0.985	0.985
λ = 0.1, $C_{o\ (MWCNTs)}$ = 5 mg L^{-1}, $C_{o\ (SDBS)}$ = 10 mg L^{-1}												
3	M1	−231.00	0.211	0.000	9.277	0.134	0.000	0.067	0.009	0.943	0.689	0.968
S5	M2	−231.10	0.211	4.16E-04	9.277	0.134	0.014	0.067	0.009	0.944	0.689	0.968
S5	M3	−211.70	27.450	0.625	19.910	0.384	296.700	0.362	0.200	0.944	0.971	0.703
λ = 0.3, $C_{o\ (MWCNTs)}$ = 5 mg L^{-1}, $C_{o\ (SDBS)}$ = 10 mg L^{-1}												
3	M1	−132.20	1.800	0.000	51.430	0.131	0.000	0.070	0.008	0.963	0.139	0.962
S5	M2	1.00	1.800	0.091	51.430	0.131	0.040	0.070	0.008	0.963	0.139	0.964

Fig. No. is the number of Fig.; *SST* is the simulated model based on single-species transport of MWCNTs or SDBS; λ, the mass ratio of goethite coated quartz sand (GQS) in the porous medium; when λ = 0, the porous medium is quartz sand. *AIC* is Akaike information criterion; k_1, the first-order retention rate coefficient of MWCNTs; k_d = 1.0E-04 min^{-1}, the first-order release rate coefficient of MWCNTs; S^{max}/C_o, the normalized maximum solid phase concentration of deposited MWCNTs; k_{1s}, the first-order retention rate coefficient of SDBS; k_{ds}, the first-order release rate coefficient of SDBS; S_s^{max}/C_o, the normalized maximum solid phase concentration of deposited SDBS; Γ, the area conversion factor between MWCNTs and SDBS; Γ_s, the area conversion factor between SDBS and MWCNTs; R^2_{BTC}, R^2_{RP}, *and* $R^2_{s\ BTC}$ reflect the correlation of observed and fitted data for BTC of MWCNTs, RP of MWCNTs, and BTC of SDBS; *NA* - denotes not applicable.

min^{-1}). Similar MWCNTs transport behavior and trends in model parameters have been reported by Zhang et al. (2016b). These authors discussed mechanisms of MWCNT retention in QS and GQS in the absence of surfactant. In brief, their results indicated that nanoscale roughness played an important role in contributing to MWCNT retention in QS by reducing or eliminating the energy barrier, whereas microscopic roughness altered the lever arms for applied hydrodynamic (decreases) and resisting adhesive (increases) torques. These same factors also contributed to MWCNT retention in GQS, but additional retention occurred with increasing λ due to more electrostatically favorable sites.

Observed and simulated RPs for MWCNTs are given as normalized solid-phase concentrations (S/C_o) versus column depth in Fig. 1b. Most previous studies have reported hyper-exponential shaped RPs for MWCNTs (Kasel et al., 2013a; Kasel et al., 2013b; Wang et al., 2012b; Zhang et al., 2016a; Zhang et al., 2017), and our modeling approach which considered depth-dependent retention provided a better description of the RPs than the uniform model with $\beta = 0$ (data not shown). However, Fig. 1b shows nonmonotonic RPs for the MWCNTs. Nonmonotonic RPs have previously been observed for other colloids and attributed to a number of potential factors such as variations in the pore-scale velocity distribution (Bradford et al., 2011), solid phase colloid migration (Yuan and Shapiro, 2011), colloid distribution properties (Bradford et al., 2006; Tong et al., 2008), competitive blocking (Becker et al., 2015), and reversible blocking (Leij et al., 2016). Competitive blocking does not occur in the single-species transport experiments, solid phase migration is expected to be more difficult for rod shaped MWCNTS than spherical colloids, and the MWCNT detachment rate was determined to be very small. Consequently, the most likely of these explanations are common variations in the pore-scale velocity or MWCNT distribution properties.

Arrival of the SDBS BTCs in Fig. 1c was slightly delayed in comparison to the conservative tracer, approached a constant C/C_o value of 1, and then exhibited considerable amounts of low concentration tailing. The SDBS BTC for $\lambda = 0.1$ had a greater delay and concentration tailing than that for the $\lambda = 0$ condition. The SDBS effluent mass balance (M_{surf}) slightly decreased from 95.5% to 92.8% (Table 1) as λ increased from 0 to 0.1, which was expected from batch experiments (Fig. S3). This observation suggests that some of the SDBS was irreversibly sorbed onto the sand surfaces, and this amount increased with λ. The SDBS BTCs were well described using the model that considered retention, release, and blocking ($R^2 > 0.986$). Both k_{1s} and S_s^{max}/C_o increased with λ. Similar to MWCNTs, blocking played an important role in SDBS transport. In contrast to MWCNTs, SDBS had much higher release rates ($k_{ds} = 0.2$ min^{-1}), which indicates significant amounts of reversible retention.

3.3. Simultaneous transport of MWCNTs and SDBS in QS

Fig. 2 presents observed and simulated (M1 model) BTCs (Fig. 2a) and RPs (Fig. 2b) for MWCNTs in QS when the SDBS concentration equaled 0, 10, and 50 mg L^{-1}. The experimental information and mass recoveries from the effluent and solid phase are presented in Table 1. The value of M_{eff} strongly increased from 17.5% to 90.5% (Table 1) as the input concentration of SDBS increased from 0 mg L^{-1} to 50 mg L^{-1}. Similar to results of Tian et al. (2011) and Lu et al. (2013), the MWCNTs were highly mobile in the presence of 10 or 50 mg L^{-1} SDBS with values of M_{eff} equal to 87.2% and 90.5%, respectively. In addition, the RPs of MWCNTs became hyper-exponential in the presence of SDBS, whereas they were nonmonotonic in the absence of SDBS. Consequently, both BTCs and RPs of MWCNTs demonstrated that SDBS can enhance MWCNTs transport in QS. Potential explanations will be discussed below.

Observed and simulated (M1) BTCs for 10 and 50 mg L^{-1} SDBS in the QS are given in Fig. 2c. Similar to Fig. 1c in the absence of MWCNTs, SDBS was highly mobile (M_{surf}>91.6%) in the QS that contained retained MWCNTs. Values of M_{surf} were comparable to those in the absence of MWCNTs (95.5%). Consequently, only a small fraction of SDBS was adsorbed onto the MWCNT surfaces (<3.9%) and to the QS (<4.5%), although much higher adsorption per unit mass occurs for MWCNTs than QS (Fig. S3). Similar to Fig. 1c, the BTCs were slightly delayed in comparison to the conservative tracer, approached a constant C/C_o value of 1, and then exhibited considerable amounts of low concentration tailing. However, the delay in breakthrough decreased with increasing SDBS concentration, presumably due to a more rapid filling of available retention sites. The values of M_{surf} increased from 91.6% to 95% as the input concentration of SDBS increased from 10 to 50 mg L^{-1} for a similar reason.

Several reasons can explain the enhancement of MWCNT transport in the presence of SDBS. Sorption of SDBS onto the surface of the QS and the MWCNTs (Fig. S3) produces a more negative surface charge (Fig. S1), which would increase the electrostatic repulsion between MWCNTs in suspension and with the QS. In addition, sorption of organics onto surfaces has been reported to enhance suspension stability and diminish retention as a result of steric repulsion (And and Sticher, 1997; Flynn et al., 2012; Yang et al., 2014), alteration of nanoscale roughness properties (Bradford et al., 2017), and/or competitive blocking (Becker et al., 2015; Lin et al., 2012; Wang et al., 2012c). Note that the M1 model provided a reasonable description of the transport and retention behavior of MWCNTs and SDBS in Fig. 2. Table 2 summarizes fitted and statistical parameters for the M1, M2, and M3 models (simulation results are shown in Fig. S4) that allowed for no, limited, and maximum competitive blocking, respectively. Values of R^2 and the Akaike information criterion (AIC) (Akaike, 1974) indicate that the M1 model was preferred. Consequently, competitive blocking is not expected to play the dominant role in enhancing MWCNT transport in the presence of SDBS. A viable alternative explanation is due to alternation of interaction energies between MWCNTs and QS by SDBS sorption. In particular, SDBS sorption can increase the energy barrier to MWCNTs interactions by increasing electrostatic and/or steric interactions, or by eliminating the energy barrier and creating a shallow (reversible) primary minimum through modification of the surface roughness properties. In support of this hypothesis the values of k_1 and S^{max}/C_o for the M1 model were greatly reduced in the presence than the absence of SDBS (Table 2).

3.4. Simultaneous transport of MWCNTs and SDBS in GQS

Significant mobility of MWCNTs was observed in the QS in the presence of SDBS (Fig. 2a and b). Additional experiments were conducted to better understand the effect of SDBS on MWCNT transport in the presence of goethite coatings. Fig. 3 presents observed and simulated (M1 model) BTCs (Fig. 3a) and RPs (Fig. 3b) for MWCNTs in sand with $\lambda = 0$, 0.1, and 0.3 when the SDBS concentration equaled 10 mg L^{-1}. The experimental conditions and mass recoveries are presented in Table 1, and the M1 model and statistical parameters are given in Table 2.

The value of M_{eff} strongly decreased from 87.2% to 0.3% as λ increased from 0 to 0.3 when the SDBS concentration was 10 mg L^{-1} (Table 1). This observation indicates that geothite coatings had a large influence on MWCNT transport even in the presence of SDBS. Table 2 indicates that the M1 model provided a good description of the BTCs for MWCNTs in sand with different values of λ and SDBS. Values of k_1 and S^{max}/C_o increased with λ (Table 2), indicating that GQS was a preferential retention site even in the presence of SDBS. Blocking was observed in the MWCNTs BTCs

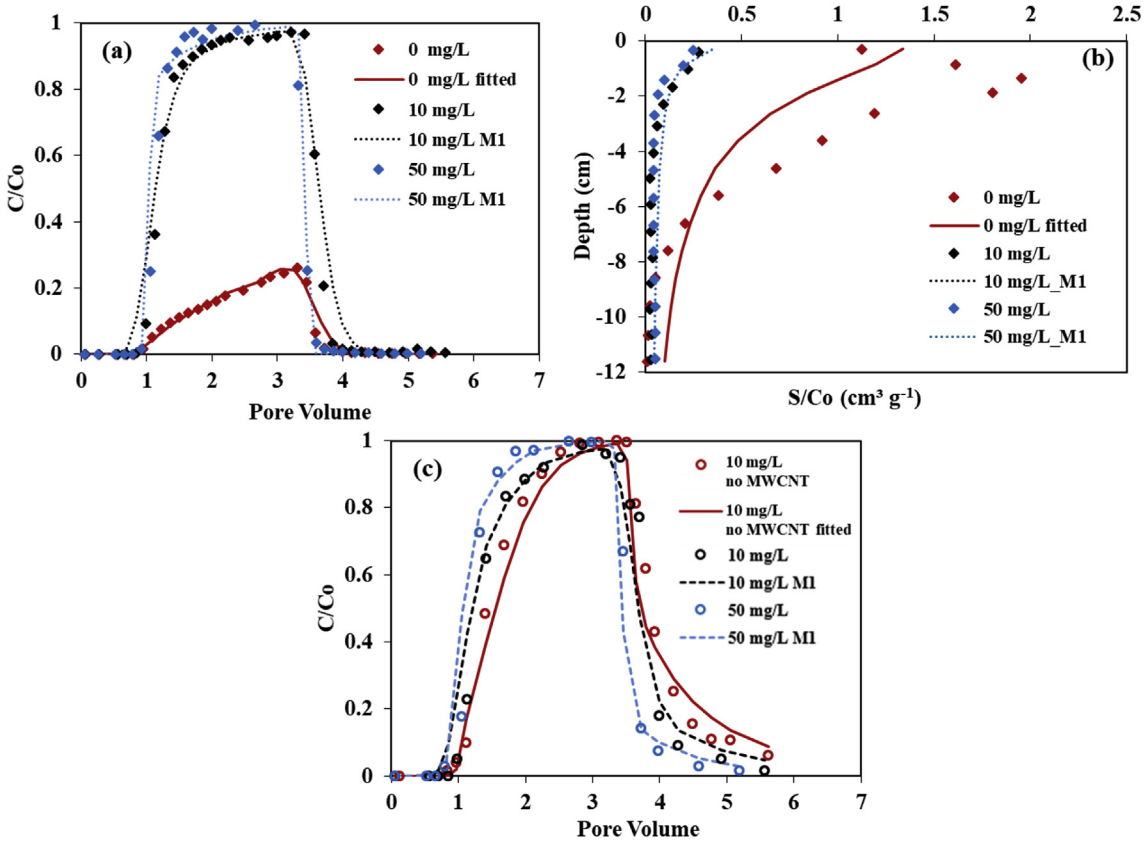

Fig. 2. Observed and fitted BTCs (a and c) and RPs (b) of MWCNTs and SDBS with or without additional SDBS or MWCNTs in quartz sand (λ = 0). (a) BTCs of MWCNTs with adding 0, 10, and 50 mg L^{-1} of SDBS; (b) RPs of MWCNTs with adding 0, 10, and 50 mg L^{-1} of SDBS; (c) BTCs of SDBS without MWCNTs, and with MWCNTs at 10 and 50 mg L^{-1} of SDBS. The input concentration of MWCNTs was 5 mg L^{-1}. The ionic strength was 1 mM KCl. The Darcy velocity is 0.71–0.73 cm min^{-1}.

(Fig. 3a), and MWCNTs exhibited greater delay in breakthrough with increasing λ because they take longer to fill a larger value of S^{max}/C_o. The RPs were hyper-exponential in shape and well described using the M1 model when λ = 0 and 0.1 (Fig. 3b). In contrast, the RP for the λ = 0.3 condition was non-monotonic in shape and exhibited a peak value at a depth of about −5 cm that was not accurately captured by the M1 model. A non-monotonic RP was also observed for the λ = 0 and 0.1 systems in the absence of SDBS (Fig. 1b), which was attributed to variations in the pore-scale velocity distribution (Bradford et al., 2011) and/or MWCNT distribution properties (Bradford et al., 2006; Tong et al., 2008). In addition to these processes, competitive blocking (Becker et al., 2015) and reversible blocking (Leij et al., 2016) are expected to contribute to the development of non-monotonic RPs in the presence of SDBS and this likely explains the peak MWCNT value at a greater depth.

Comparison of results for λ = 0.1 in the presence (Fig. 3a and b) and absence (Fig. 1a and b) of SDBS reveals that the surfactant greatly enhanced the transport of MWCNT (e.g., M_{eff} increased from 2.4% to 64.2%). Similar to QS (Fig. 2), this enhanced transport of MWCNTs is attributed to alteration of the interaction energy by SDBS sorption (e.g., increasing electrostatic and/or steric interactions, or by creating reversible interactions on rough surfaces).

The value of M_{surf} for SDBS was equal to 91.6%, 86.4%, and 84.2% when λ = 0, 0.1, and 0.3, respectively (Table 1). This decrease in M_{surf} with an increase in λ reflects the presence of more irreversible retention sites for SDBS on a geothite surface and/or on retained MWCNTs (which also increased with an increase in λ). The observed and simulated BTCs for SDBS in sand with λ = 0, 0.1, and 0.3 are shown in Fig. 3c. The BTCs for SDBS exhibited similar behavior to those shown in Figs. 1c and 2c, and were well described using the M1 model (Table 2). Analogous to the SDBS in QS (Figs. 1c and 2c), the values of k_{1s} and S_s^{max}/C_o for the M1 model were reduced in the presence than the absence of MWCNTs (Table 2). Similar to simultaneous transport of MWCNTs and SDBS in QS, the fitted and statistical parameters from M2 and M3 models in GQS are summarized in Table 2 and shown in Fig. S5.

3.5. Remobilization of retained MWCNTs in GQS by SDBS injection

An additional experiment was conducted to investigate the potential for injection of 10 mg L^{-1} of SDBS to remobilize MWCNTs that were initially retained in sand with λ = 0.1 in the absence of surfactant (Fig. 4). The initial retention phase for MWCNTs was conducted in an analogous fashion to Fig. 1 and this λ = 0.1 dataset was also included in Fig. 4 for comparison purposes. The solution chemistry sequence for remobilization was meant to simulate the process of using SDBS to remediate soil contaminated by MWCNTs. Even though the mobility of MWCNTs was limited in sand with λ = 0.1 (M_{eff} = 2.4%), it still appeared again in the outflow at low levels after SDBS injection (Fig. 4a). In addition, the concentrations of retained MWCNTs were also obviously decreased in the top layers and increased in the deeper layers of the column due to the SDBS elution (Fig. 4b). This shift demonstrated that injection of SDBS facilitated the remobilization of MWCNTs.

Mass balance information in Table 1 indicates that co-injection of MWCNTs and SDBS produced a much greater recovery in the effluent (M_{eff} = 64.2%) in comparison to sequential injection of MWCNTs and SDBS (M_{eff} = 2.5%). The high recovery of MWCNTs during co-injection was attributed in sections 3.2 and 3.2 to the

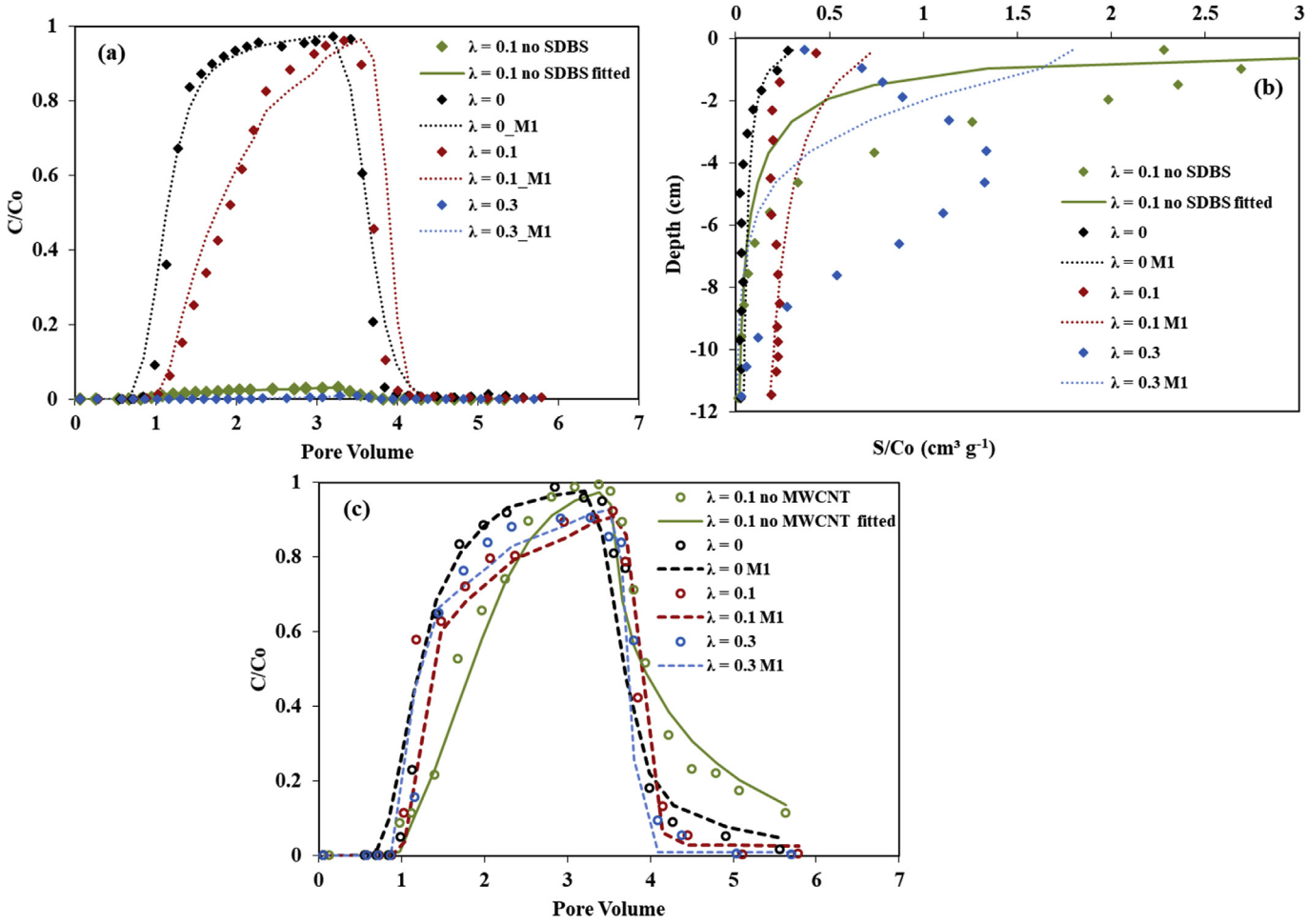

Fig. 3. Observed and fitted BTCs (a and c) and RPs (b) of MWCNTs and SDBS in porous media at different λ. (a) BTCs of MWCNTs without adding SDBS at λ = 0.1, and with adding SDBS at λ = 0, 0.1, and 0.3; (b) RPs of MWCNTs without adding SDBS at λ = 0.1, and with adding SDBS at λ = 0, 0.1, and 0.3; (c) BTCs of SDBS in the absence of MWCNTs at λ = 0.1, and presence of MWCNTs at λ = 0, 0.1, and 0.3. The input concentrations of MWCNTs and SDBS were 5 and 10 mg L^{-1}, respectively. The ionic strength was 1 mM KCl. The Darcy velocity is 0.71–0.73 cm min^{-1}.

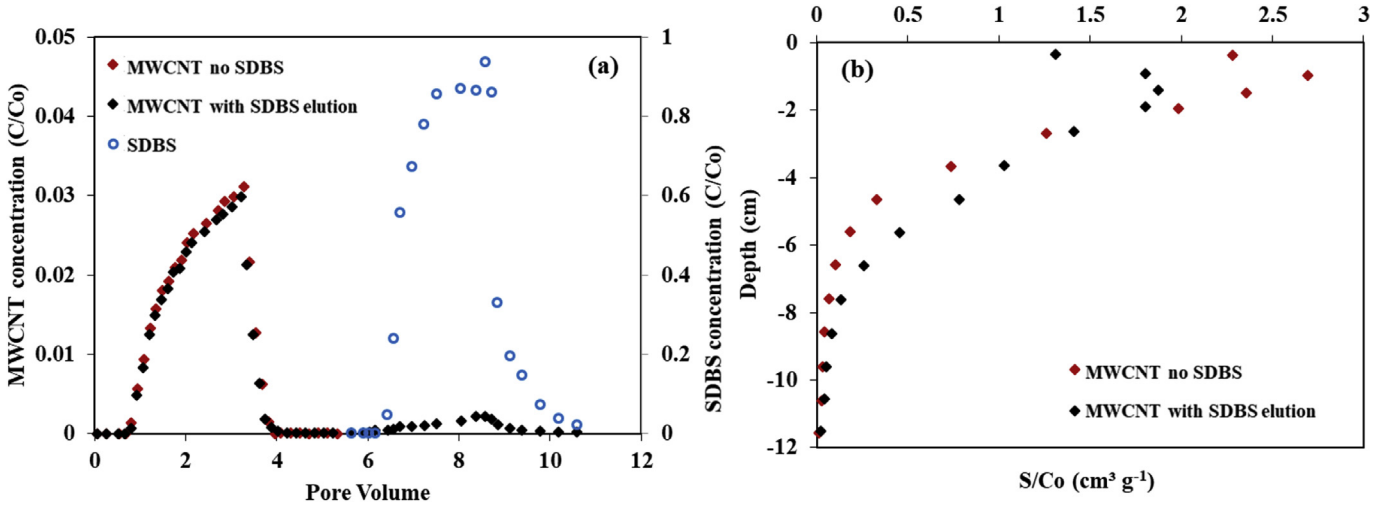

Fig. 4. Observed BTCs (a) and RPs (b) of MWCNTs and SDBS without SDBS and with SDBS elution at λ = 0.1. Fig. (4a) has two vertical axes. The left axis shows the relative MWCNTs concentration, while the right axis shows the relative SDBS concentration. The input concentration of MWCNTs and SDBS was 5 and 10 mg L^{-1}, respectively. The ionic strength was 1 mM KCl. The Darcy velocity is 0.71–0.73 cm min^{-1}.

influence of SDBS adsorption on the interaction energy between MWCNTs and the sand (e.g., increases in electrostatic and steric interactions, and/or alteration of surface roughness properties). The results from the sequential injection of MWCNTs and SDBS (Fig. 4) suggest that it is much more difficult to alter the interaction energy and promote release once the MWCNTs have been retained. This is due to the difference in the energy barrier for retention and release of MWCNTs. In particular, the initial retention of MWCNTs depends on the energy barrier to the minimum, which was eliminated on electrostatically favorable surfaces like goethite. Conversely, the release of MWCNTs depends on the difference in the magnitude of the minimum and the energy barrier height. Note that the depth of the primary minimum is expected to be large on goethite surfaces that are smooth. Consequently, the energy barrier to release is expected to be much larger than for retention on goethite coated surfaces. Furthermore, adsorption of SDBS increases the energy barrier to detachment by increasing electrostatic (Fig. S1) and steric interactions (And and Sticher, 1997; Flynn et al., 2012; Yang et al., 2014). Conversely, alteration of surface roughness properties by SDBS adsorption can decrease the depths of both primary and secondary minimum, and thereby decrease the energy barrier to detachment (Bradford et al., 2017). Diffusive release of MWCNT from a shallow minimum on rough goethite coated sand may occur when the energy barrier to detachment is decreased to less than a few dimensionless energy units.

The transport behavior of SDBS following the pulse application of MWCNT was generally consistent with previously discussed results for SDBS in sand with $\lambda = 0.1$ in Fig. 1 (absence of MWCNTs) and 3 (simultaneous injection of MWCNTs and SDBS). However, the value of M_{surf} for SDBS on sand with $\lambda = 0.1$ was found to depend on the presence of MWCNTs and the injection sequence. In particular, the value of M_{surf} equaled 92.8% in the absence of MWCNTs (Fig. 1), 86.4% when MWCNTs and SDBS were simultaneously injected (Fig. 3), and 80% when MWCNTs and SDBS were sequentially injected (Fig. 4). This decrease in M_{surf} corresponds to increasing amounts of MWCNT retention in these systems (Table 1) with a high sorption capacity of MWCNTs for SDBS (Fig. S3).

4. Conclusions

The presence of the anionic surfactant SDBS in sewer or wastewater treatment effluent will greatly influence the co-transport of MWCNTs in chemically heterogeneous sand. Modeling results indicated that competitive blocking only played a secondary role in enhancing the transport of MWCNTs by SDBS. Rather, SDBS adsorption onto the surfaces of quartz and goethite minerals, and especially MWCNTs decreased their zeta potentials and/or even reversed the charge of positively charged minerals. This surface modification will enhance the electrostatic and/or steric repulsion, and alter the nanoscale surface roughness properties that strongly reduce the adhesion of MWCNTs to solid surfaces. Both of these factors will greatly enhance the transport and alter the shape of retention profiles for MWCNTs in chemically heterogeneous media in the presence of SDBS. It is logical to anticipate that surface modification by anionic surfactants may similarly influence the fate of other colloids and nanoparticles. This process may potentially be exploited to deliver selected colloids or nanoparticles to desired locations in the subsurface for remediation purposes (e.g., zero valent iron), or inadvertently increase the risk of colloid contamination (e.g., pathogenic microorganisms). In contrast to co-injection, sequential injection of MWCNTs and SDBS pulses produced only a limited enhancement in the remobilization of retained MWCNTs presumably due to a greater energy barrier for release than retention. This implies that discharge of anionic surfactants will have a greater impact on the transport of colloids in the aqueous phase than on the release of retained colloids. These findings provide new insights on the effects of anionic surfactants on the transport, retention, and release of colloids and nanoparticles in porous media, and their role in remediation scenarios and contamination risks.

Acknowledgements

Funding was provided by the National Key R&D Program of China (Project No. SQ2018YFD080023), the 111 Project (Project No. B18060), the National Natural Science Foundation of China (Project No. 41701547), and China Postdoctoral Science Foundation (Project No. 2017M612806 and 2018T110909). The authors would like to acknowledge Stephan Köppchen for bromide measurement. Thanks to Herbert Philipp and Claudia Walraf for their technical assistance.

Appendix A. Supplementary data

Supplementary data to this article can be found online at https://doi.org/10.1016/j.envpol.2019.01.106.

References

Adamczyk, Z., Siwek, B., Zembala, M., Belouschek, P., 1994. Kinetics of localized adsorption of colloid particles. Adv. Colloid Interface Sci. 48 (94), 151–280.
Akaike, H., 1974. A new look at statistical model identification. IEEE Trans. Automat. Contr. AC19 (6), 716–723.
Alvarezsilva, M., Uribesalas, A., Mirnezami, M., Finch, J.A.J.M.E., 2010. The point of zero charge of phyllosilicate minerals using the Mular-Roberts titration technique, 23 (5), 383–389.
And, R.K., Sticher, H., 1997. Transport of humic-coated iron oxide colloids in a sandy Soil: influence of Ca^{2+} and trace metals. Environ. Sci. Technol. 31 (12), 3497–3504.
Becker, M.D., Wang, Y., Pennell, K.D., Abriola, L.M., 2015. A multi-constituent site blocking model for nanoparticle and stabilizing agent transport in porous media. Environ. Sci.: Nano 2 (2), 155–166.
Bradford, S.A., Kim, H., Shen, C., Sasidharan, S., Shang, J., 2017. Contributions of nanoscale roughness to anomalous colloid retention and stability behavior. Langmuir 33 (38).
Bradford, S.A., Šimůnek, J., Walker, S.L., 2006. Transport and straining of E. coli O157: H7 in saturated porous media. Water Resour. Res. 42 (12), 150–152.
Bradford, S.A., Torkzaban, S., Šimůnek, J., 2011. Modeling colloid transport and retention in saturated porous media under unfavorable attachment conditions. Water Resour. Res. 47 (10), 599–609.
Camilli, L., Pisani, C., Gautron, E., Scarselli, M., Castrucci, P., D'Orazio, F., Passacantando, M., Moscone, D., De, C.M., 2014. A three-dimensional carbon nanotube network for water treatment. Nanotechnology 25 (6), 065701.
Dillon, A.C., Jones, K.M., Bekkedahl, T.A., Kiang, C.H., Bethune, D.S., Heben, M.J., 1997. Storage of hydrogen in single-walled carbon nanotubes. Nature 386 (6623), 377–379.
Duan, X., Xu, F., Wang, Y., Chen, Y., Chang, L.J.E.A., 2018. Fabrication of a Hydrophobic SDBS-PbO 2 Anode for Electrochemical Degradation of Nitrobenzene in Aqueous Solution, vol 282, pp. 662–671.
Flynn, R.M., Yang, X., Hofmann, T., Von, d.K.F., 2012. Bovine serum albumin adsorption to iron-oxide coated sands can change microsphere deposition mechanisms. Environ. Sci. Technol. 46 (5), 2583–2591.
Gottschalk, F., Sonderer, T., Scholz, R.W., Nowack, B., 2009. Modeled environmental concentrations of engineered nanomaterials (TiO_2, ZnO, Ag, CNT, Fullerenes) for different regions. Environ. Sci. Technol. 43 (24), 9216–9222.
Guldi, D.M., Rahman, G.M., Prato, M., Jux, N., Qin, S., Ford, W., 2005. Single-wall carbon nanotubes as integrative building blocks for solar-energy conversion. Angew. Chem. Int. Ed. 44 (13), 2015–2018.
Han, Z., Zhang, F., Lin, D., Xing, B., 2008. Clay minerals affect the stability of surfactant-facilitated carbon nanotube suspensions. Environ. Sci. Technol. 42 (18), 6869.
Hassellöv, M., Readman, J.W., Ranville, J.F., Tiede, K., 2008. Nanoparticle analysis and characterization methodologies in environmental risk assessment of engineered nanoparticles. Ecotoxicology 17 (5), 344–361.
Iijima, S., 1991. Helical microtubules of graphitic carbon. Nature 354 (6348), 56–58.
Jaisi, D.P., Elimelech, M., 2009. Single-walled carbon nanotubes exhibit limited transport in soil columns. Environ. Sci. Technol. 43 (24), 9161.
Janas, D., Herman, A.P., Boncel, S., Koziol, K.K.K., 2014. Iodine monochloride as a powerful enhancer of electrical conductivity of carbon nanotube wires. Carbon 73 (7), 225–233.
Kasel, D., Bradford, S.A., Šimůnek, J., Heggen, M., Vereecken, H., Klumpp, E., 2013a. Transport and retention of multi-walled carbon nanotubes in saturated porous

media: effects of input concentration and grain size. Water Res. 47 (2), 933.
Kasel, D., Bradford, S.A., Simůnek, J., Pütz, T., Vereecken, H., Klumpp, E., 2013b. Limited transport of functionalized multi-walled carbon nanotubes in two natural soils. Environ. Pollut. 180 (3), 152–158.
Leij, F.J., Bradford, S.A., Sciortino, A., 2016. Analytic solutions for colloid transport with time- and depth-dependent retention in porous media. J. Contam. Hydrol. 195, 40.
Li, C., Schäffer, A., Séquaris, J.M., László, K., Tóth, A., Tombácz, E., Vereecken, H., Ji, R., Klumpp, E., 2012. Surface-associated metal catalyst enhances the sorption of perfluorooctanoic acid to multi-walled carbon nanotubes. J. Colloid Interface Sci. 377 (1), 342.
Liang, Y., Bradford, S.A., Šimůnek, J., Vereecken, H., Klumpp, E., 2013. Sensitivity of the transport and retention of stabilized silver nanoparticles to physicochemical factors. Water Res. 47 (7), 2572–2582.
Lin, H., Hong, Z., Guo, H., Yu, L., 2008. Microwave-absorbing properties of Co-filled carbon nanotubes. Mater. Res. Bull. 43 (10), 2697–2702.
Lin, S., Cheng, Y., Liu, J., Wiesner, M.R., 2012. Polymeric coatings on silver nanoparticles hinder autoaggregation but enhance attachment to uncoated surfaces. Langmuir the Acs J. Surface. Colloid. 28 (9), 4178–4186.
Liu, X., O'Carroll, D.M., Petersen, E.J., Huang, Q., Anderson, C.L., 2009. Mobility of multiwalled carbon nanotubes in porous media. Environ. Sci. Technol. 43 (21), 8153–8158.
Lu, Y., Xu, X., Yang, K., Lin, D., 2013. The effects of surfactants and solution chemistry on the transport of multiwalled carbon nanotubes in quartz sand-packed columns. Environ. Pollut. 182 (6), 269–277.
Lu, Y., Yang, K., Lin, D., 2014. Transport of surfactant-facilitated multiwalled carbon nanotube suspensions in columns packed with sized soil particles. Environ. Pollut. 192, 36–43.
Matarredona, O., Rhoads, H., Li, Z., Harwell, J.H., Balzano, L., Resasco, D.E., 2003. Dispersion of single-walled carbon nanotubes in aqueous solutions of the anionic surfactant NaDDBS. J. Phys. Chem. B 107 (48), 13357–13367.
Matthijs, E., Holt, M.S., Kiewiet, A., Rijs, G.B.J., 1999. Environmental monitoring for linear alkylbenzene sulfonate, alcohol ethoxylate, alcohol ethoxy sulfate, alcohol sulfate, and soap. Environ. Toxicol. Chem. 18 (11), 2634–2644.
Mauter, M.S., Elimelech, M., 2008. Environmental applications of carbon-based nanomaterials. Environ. Sci. Technol. 42 (16), 5843.
OECD, 2006. Test No. 106: adsorption – desorption using a batch equilibrium method. OECD Guidel. Test. Chem. 1 (1), 1–44.
Pan, B., Xing, B., 2012. Applications and implications of manufactured nanoparticles in soils: a review. Eur. J. Soil Sci. 63 (4), 437–456.
Parks, G.A., 1965. The isoelectric points of solid oxides, solid hydroxides, and aqueous hydroxo complex systems. Chem. Rev. 65 (2).
Pauluhn, J., 2010. Multi-walled carbon nanotubes (Baytubes®): approach for derivation of occupational exposure limit. Regul. Toxicol. Pharmacol. 57 (1), 78–89.
Pecora, R., 2000. Dynamic light scattering measurement of nanometer particles in liquids. J. Nanoparticle Res. 2 (2), 123–131.
Šimůnek, J., Genuchten, M.T.V., Šejna, M., 2008. Development and applications of the HYDRUS and STANMOD software packages and related codes. Vadose Zone J. 72 (9), 587–600.
Tan, X., Fang, M., Chen, C., Yu, S., Wang, X., 2008. Counterion effects of nickel and sodium dodecylbenzene sulfonate adsorption to multiwalled carbon nanotubes in aqueous solution. Carbon 46 (13), 1741–1750.
Tian, Y., Gao, B., Ziegler, K.J., 2011. High mobility of SDBS-dispersed single-walled carbon nanotubes in saturated and unsaturated porous media. J. Hazard Mater. 186 (2–3), 1766–1772.
Tong, M., Ma, H., Johnson, W.P., 2008. Funneling of flow into grain-to-grain contacts drives Colloid–Colloid aggregation in the presence of an energy barrier. Environ. Sci. Technol. 42 (8), 2826–2832.
Wang, D., Bradford, S.A., Harvey, R.W., Gao, B., Cang, L., Zhou, D., 2012a. Humic acid facilitates the transport of ARS-labeled hydroxyapatite nanoparticles in iron oxyhydroxide-coated sand. Environ. Sci. Technol. 46 (5), 2738–2745.
Wang, Y., Kim, J.H., Baek, J.B., Miller, G.W., Pennell, K.D., 2012b. Transport behavior of functionalized multi-wall carbon nanotubes in water-saturated quartz sand as a function of tube length. Water Res. 46 (14), 4521–4531.
Wang, Y., Li, Y., Costanza, J., Abriola, L.M., Pennell, K.D., 2012c. Enhanced mobility of fullerene (C_{60}) nanoparticles in the presence of stabilizing agents. Environ. Sci. Technol. 46 (21), 11761.
Wei, X., Wang, Y., Bergsträßer, R., Kundu, S., Muhler, M., 2007. Surface characterization of oxygen-functionalized multi-walled carbon nanotubes by high-resolution X-ray photoelectron spectroscopy and temperature-programmed desorption. Appl. Surf. Sci. 254 (1), 247–250.
Yang, J., Bitter, J.L., Smith, B.A., Fairbrother, D.H., Ball, W.P., 2013. Transport of oxidized multi-walled carbon nanotubes through silica based porous media: influences of aquatic chemistry, surface chemistry, and natural organic matter. Environ. Sci. Technol. 47 (24), 14034–14043.
Yang, X., Lin, S., Wiesner, M.R., 2014. Influence of natural organic matter on transport and retention of polymer coated silver nanoparticles in porous media. J. Hazard Mater. 264 (2), 161.
Yu, J., Grossiord, N., Koning, C.E., Loos, J., 2007. Controlling the dispersion of multi-wall carbon nanotubes in aqueous surfactant solution. Carbon 45 (3), 618–623.
Yuan, H., Shapiro, A.A., 2011. Induced migration of fines during waterflooding in communicating layer-cake reservoirs. J. Petrol. Sci. Eng. 78 (3), 618–626.
Yuan, T., Gao, B., Lei, W., Muñoz-Carpena, R., Huang, Q., 2012. Effect of solution chemistry on multi-walled carbon nanotube deposition and mobilization in clean porous media. J. Hazard Mater. 231–232 (6), 79–87.
Zhang, M., Bradford, S.A., Šimůnek, J., Vereecken, H., Klumpp, E., 2016a. Roles of cation valance and exchange on the retention and colloid-facilitated transport of functionalized multi-walled carbon nanotubes in a natural soil. Water Res. 109, 358.
Zhang, M., Bradford, S.A., Šimůnek, J., Vereecken, H., Klumpp, E., 2016b. Do goethite surfaces really control the transport and retention of multi-walled carbon nanotubes in chemically heterogeneous porous media? Environ. Sci. Technol. 50 (23), 12713.
Zhang, M., Engelhardt, I., Šimůnek, J., Bradford, S.A., Kasel, D., Berns, A.E., Vereecken, H., Klumpp, E., 2017. Co-transport of chlordecone and sulfadiazine in the presence of functionalized multi-walled carbon nanotubes in soils. Environ. Pollut. 221, 470–479.
Zhang, S., Shao, T., Kose, H.S., Karanfil, T., 2010. Adsorption of aromatic compounds by carbonaceous adsorbents: a comparative study on granular activated carbon, activated carbon fiber, and carbon nanotubes. Environ. Sci. Technol. 44 (16), 6377.